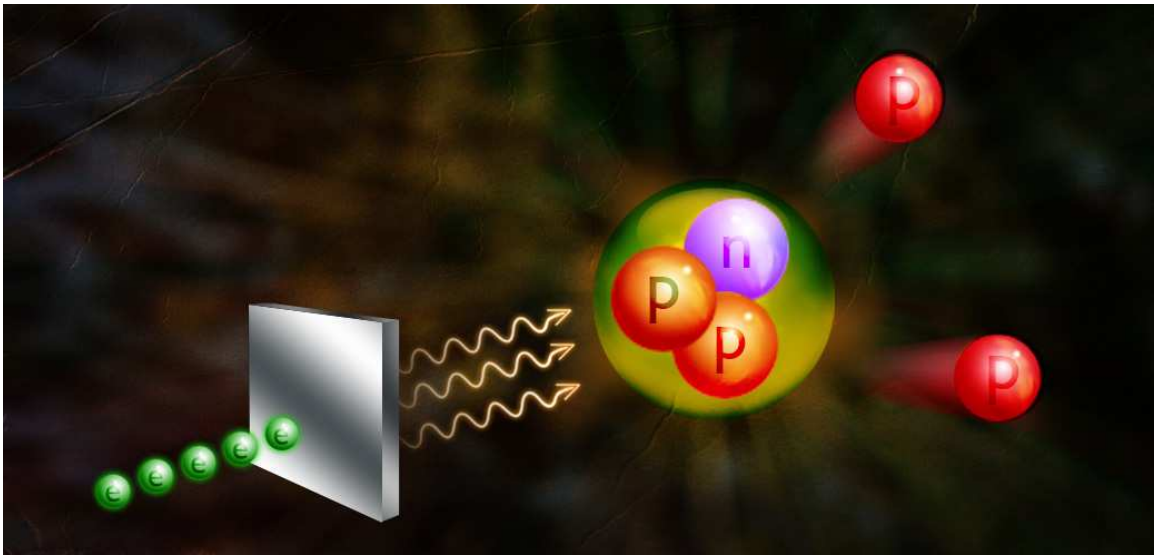


Hard photodisintegration of ${}^3\text{He}$ into *pp* and *pn* pairs

The Jefferson Lab Hall A Collaboration



X. Zhan
Argonne National Laboratory, Argonne, Illinois, 60439, USA

C. Granados, P. Markowitz and M. Sargsian
Florida International University, Miami, FL 33199 USA

G. Ron
Hebrew University of Jerusalem, Jerusalem, Israel

F. Garibaldi
INFN, gruppo collegato Sanità and Istituto Superiore di Sanità,
Department TESA, I-00161 Rome, Italy

A. Camsonne, D.W. Higinbotham (spokesperson), R. Michaels and B. Sawatzky
Jefferson Lab, Newport News, VA 23606 USA

S. Gilad
Massachusetts Institute of Technology, Cambridge, MA 02139 USA

M. H. Shabestari
Mississippi State University, Starkville, MS 39762 USA

L. Weinstein
Old Dominion University, Norfolk, VA 23529 USA

L. El Fassi, R. Gilman (spokesperson), S. Leighton
G. Kumbartzki, R. Ransome and Y. Zhang
Rutgers University, Piscataway, NJ 08854-8019 USA

A.J. Sarty
St. Mary's University, Halifax, Nova Scotia B3H 3C3 Canada

N. Bubis, O. Hen, I. Korover, E. Piassetzky,
I. Pomerantz (spokesperson and contact person) and R. Shneor
Tel Aviv University, Tel Aviv, Israel

Y. Ilieva and S. Strauch (spokesperson)
University of South Carolina, Columbia, South Carolina 29208, USA

C. Hanretty, R. Lindgren, B.E. Norum
University of Virginia, Charlottesville, Virginia 22904, USA

Executive Summary

Extensive studies of hard two-nucleon photodisintegration over the past two decades have probed the limits of meson-baryon descriptions of nuclear reactions, and the effects of the underlying quark-gluon degrees of freedom.

Cross sections for deuteron photodisintegration into a proton and neutron produced at large center of mass angles are available for photon energies up to 5 GeV. For energies up to 3 (2.5) GeV there are also complete angular distributions (recoil polarizations). Recently JLab experiment E03-101 extended these studies by measuring, for the first time, the hard photodisintegration of two-protons using ^3He target.

These “first generation” experiments indicate unambiguously the onset of quark-constituent dynamics in the hard photodisintegration process, making it one of the few nuclear reactions which lies beyond the limits of description within the meson-baryon framework of strong interactions.

The existing data and theory, however, are insufficient to determine if the large transverse momentum final state nucleons are due to break-up of a pre-existing, highly correlated, two-baryon system, or if they are formed due to hard scattering in the final state of the reaction.

Identifying the source of the large transverse momentum nucleons from nuclei is the main motivation of the *second* generation of hard-break-up experiments.

These experiments envision comparative studies of pn and pp breakup from the $A = 3$ nucleus, measurement of light-cone and transverse momentum distribution of the center of mass of the two large- p_T nucleons, extension of the measurements to large energies, and probing different polarization observables of hard photodisintegration. A new generation of experiments will extend the measurements to hard-photodisintegration of two nucleons into two non-nucleonic baryons as well as to the virtual photon sector, which can be used for reconstruction of the impact-parameter picture of the hard break-up processes.

Taking into account the fact that previous experiments in many cases yielded unexpected results that influenced the planning of subsequent experiments, we propose the strategy of a step-by-step investigation in which *several short-run-time* experiments will focus on specific aspects of “second” generation measurements (see also Appendix B).

As a *first step* in this process, we intend to extend our recent measurements of hard photodisintegration reactions with ^3He . In particular, we pro-

pose comparative measurements of pp and pn photodisintegration of ${}^3\text{He}$ at large center of mass angles, with identification of the third low-momentum nucleon as a spectator to the hard reaction. Within this setup we propose to carry out:

1. Measurement of the light-cone (α_n) momentum distribution as a function of the transverse momentum (p_{Tn}) of the spectator neutron and as a function of the transverse momentum (p_{Tp}) (or equivalently c.m. angle) of the proton in the hard ${}^3\text{He}(\gamma, pp)n$ photodisintegration reaction. These measurements will enable us to determine whether the high transverse momentum originates from *initial-state correlations* or *final-state hard rescattering*, and how this distribution varies with kinematics.
2. Measurements of the cross sections of both $\gamma^3\text{He} \rightarrow pp(n)$ and $\gamma^3\text{He} \rightarrow pn(p)$ reactions will address the issue of the small measured cross section ratio of $\gamma^3\text{He} \rightarrow pp(n)$ to $\gamma d \rightarrow pn$. The understanding of the source of this suppression will provide additional constraints on the determination of the origin of high- p_T nucleons in the photodisintegration process.

The total beam time request is for 10 days. No new equipment and no special setup or development time are required. We will utilize our experience gained from the recent JLab experiment E03-101. The measurement does not require high quality beam and can be performed during the initial stages of the 12 GeV setup.

1 Scientific background and motivation

1.1 Overview

We define a hard photodisintegration of a nucleon pair as a process in which a high energy photon is absorbed by a nucleon pair and as a result the pair is disintegrated by emitting two nucleons with large transverse momenta, greater than about 1 GeV/c. As defined in this process, the magnitudes of Mandelstam parameters s and t (the square of the total energy in the c.m. frame and the four-momentum transfer from the photon to the nucleon) are much larger than the nucleon masses.

Extensive studies of high-energy deuteron photodisintegration over the past two decades [1–8], have probed the limits of meson-baryon descriptions of photo-nuclear reactions and demonstrated unambiguously the relevance of the underlying quark-gluon degrees of freedom to the energy-scaling properties of the reaction.

At low photon energies, up through the Δ -resonance region, photodisintegration of the deuteron is well understood within the meson-baryon picture of nuclear interactions, although certain detailed problems remain to be solved [9–12]. Above ~ 1 GeV photon energies, deuteron photodisintegration cross sections have been shown to scale with s^{-11} , as expected from the constituent counting rule [8, 13–16], in which nucleon wave functions are dominated by the minimal-Fock component of the quark-parton wave function.

SLAC and early JLab deuteron photodisintegration measurements focused on the observation of energy scaling. Subsequent JLAB experiments were able for the first time to measure complete angular distributions [5–7] as well as polarization observables [17, 18] in the kinematics where the s^{-11} scaling is established. The very first high-energy experiments demonstrated a clear angular asymmetry around $\theta_{cm} = 90^\circ$, indicating the importance of interference between isosinglet and isotriplet channels of pn production. A rather surprising sizable asymmetry observed for the final-state proton indicates that the leading quark in the reaction carries most of the incoming photon polarization.

The next development in the JLAB experiments was the extension of hard photodisintegration to the two-proton channel. Experiment E03-101 determined hard photoproduction of two large p_{Tp} protons from ^3He targets, with the momentum of recoil neutrons restricted to 100 MeV/c. The main

motivation of this experiment was the extension of the scope of the hard photoproduction reactions for which the validity of different theoretical approaches can be verified unambiguously (Sec. 1.3). These experiment combined with the low energy measurement from Hall B experiment produced several surprising results, particularly evidence of resonating structure at low energies and strong suppression of pp production as compared to that of pn . The ${}^3\text{He}(\gamma, pp)n$ experiments demonstrated also that the availability of the recoil neutron gives an additional handle in probing the different aspects of hard disintegration process.

1.2 Theoretical Studies

One of the most interesting aspects of theoretical studies of hard photodisintegration reactions was the fact that one needs to go beyond the conventional picture of meson-baryon interactions in order to be in agreement with the observed features of the reaction, such as the s^{-11} scaling of the differential cross section.

Two distinct theoretical approaches have been developed to describe hard-photodisintegration of the deuteron. One approach [19–22] is based on the assumption that two large- p_T nucleons are preexisting components of the deuteron wave function, and are disintegrated by the absorption of the incoming photon. The second group of models [23–28] assume that high- p_T nucleons are produced due to hadronic interactions in the final state of the reaction. All these models contained hard scattering, in the initial or in the final state of the reaction, and therefore correctly predicted the s^{-11} scaling of the differential cross section.

The interesting feature of the hard scattering in both approaches is that the scattering amplitude that is related to the preexisting high p_T wave function is real while the one related to the hard rescattering approximation is predominantly imaginary [25, 29]. As a result, the amplitudes of these two scenarios for hard photodisintegration do not interfere and the interpretation of the experimental data should be more straightforward, even in the case that both are present at similar levels.

Three theoretical models presently allow a quantitative description of the reaction. Verification of the validity of any of these models would help to understand the actual dynamics of hard photodisintegration.

Reduced Nucleon Amplitude Approximation: The reduced nuclear amplitude (RNA) formalism [19] attempts to incorporate some of the soft

physics not described by pQCD by using experimentally determined nucleon form factors to describe the gluon exchanges within the nucleons. It neglects diagrams in which gluon exchanges between the nucleons lead to non-color singlet intermediate “nucleon” states, diagrams which might be important in pQCD calculations. Analytically the scattering amplitude is expressed through the deuteron wave function at the origin, which from physics point of view means that two high p_T nucleons are pre-existing in the ground state wave function of the nucleus. Ideally, the RNA calculation should be normalized to the scaling behavior at asymptotic energies, where both yield the same result. In practice, the normalization must be to data, but at energies sufficiently large.

Hard Rescattering Model: The QCD hard rescattering model (HRM) [23] assumes that the photon is absorbed by a quark in one nucleon, followed by a high momentum transfer interaction with a quark of the other nucleon leading to the production of two nucleons with high relative momentum. Summing the relevant quark rescattering diagrams demonstrates that the nuclear scattering amplitude can be expressed as a convolution of the large angle pn scattering amplitude, the hard photon-quark interaction vertex and the low-momentum nuclear wave function. Therefore HRM assumes that source of the high p_T nucleons are the final state hard rescattering. Since the NN hard scattering amplitude can be taken from large angle NN scattering data, the HRM model allows calculation of the absolute cross section of the $\gamma \rightarrow NN$ reactions using no adjustable parameters.

Quark-Gluon String Model: The quark-gluon string model (QGS) [27,28] views the reaction as proceeding through the two steps: first photon-deuteron scatters through $(q\bar{q}) + 6q \rightarrow q5q$ channel with $q\bar{q}$ annihilating into the gluon-string which further provides the energy flow to the final state $q + (5q) \rightarrow (3q) + (3q)$ rescattering. In the leading approximation the QGS will predict s^{-12} scaling for the cross section, however for intermediate energies the model uses non-linear Regge parameterization with single reggeon exchange to obtain softer energy distributions. The $(q\bar{q}) + 6q \rightarrow q5q$ amplitude is modeled according to meson type reggeon exchange while for the $q + (5q) \rightarrow (3q) + (3q)$ the “diquark” exchange is assumed. As such the model is in between of RNA and HRM models since it assumes a small initial configuration in order the $q\bar{q}$ annihilation to take place and hard scattering in the final state in order to produce final high p_T nucleons.

Since some of above described models were normalized to the deuteron

photodisintegration data, the measured absolute cross sections of $d(\gamma, pn)$ reactions could not be used for checking the validity of the theoretical approaches.

One of the motivations for extension of photo-disintegration to the two-proton channel [30] was to discriminate these models based on their prediction of the cross section of pp relative to the pn break-up.

1.3 What was learned from previous experiments

A summary of the Jlab data at $\theta_{cm} = 90^\circ$ is given in Fig. 1 .

The figure shows the $d(\gamma, p)n$ and ${}^3\text{He}(\gamma, pp)n$ cross section at $\theta_{cm} = 90^\circ$ scaled by s^{11} . The ${}^3\text{He}(\gamma, pp)n$ events were selected with $p_n < 100$ MeV/c. The cross section is compared to predictions for the photodisintegration of both pn and pp pairs from the theoretical models discussed above [30].

For $d(\gamma, pn)$ reaction the differential cross section scales according to constituent counting prediction of s^{-11} [15, 31, 32] starting at $E_\gamma \approx 1$ GeV [6]. Already at these energies simple meson-exchange models fail to describe the data since generated intermediate state masses are well above the Δ -resonance mass [33]. The models described above generally agree with the data, however both RNA and QGS models are normalized to the measured cross section.

The measured center-of mass angular distribution for pn break-up [5, 7] are clearly asymmetric around $\theta_{cm} = 90^\circ$, being more forward peaked, a feature that qualitatively agrees with pn elastic scattering. The HRM and QGS models reproduce this asymmetry reasonably well.

High-energy, recoil-polarization experiments were also performed at JLab, with observation of a sizable asymmetry, C_z , for outgoing protons in the direction of their momenta [17, 18]. This feature too was qualitatively well described within the QGS and HRM models.

The measurement of hard photodisintegration of the ${}^3\text{He}$ nucleus into two-protons [34] yielded several new surprises:

- There is a strong apparent resonance structure at photon energies below 2 GeV that was not observed in the deuteron photodisintegration.
- The onset of s^{-11} scaling happens at a much larger photon energies (2.2 GeV) than for the deuteron case (1 GeV).

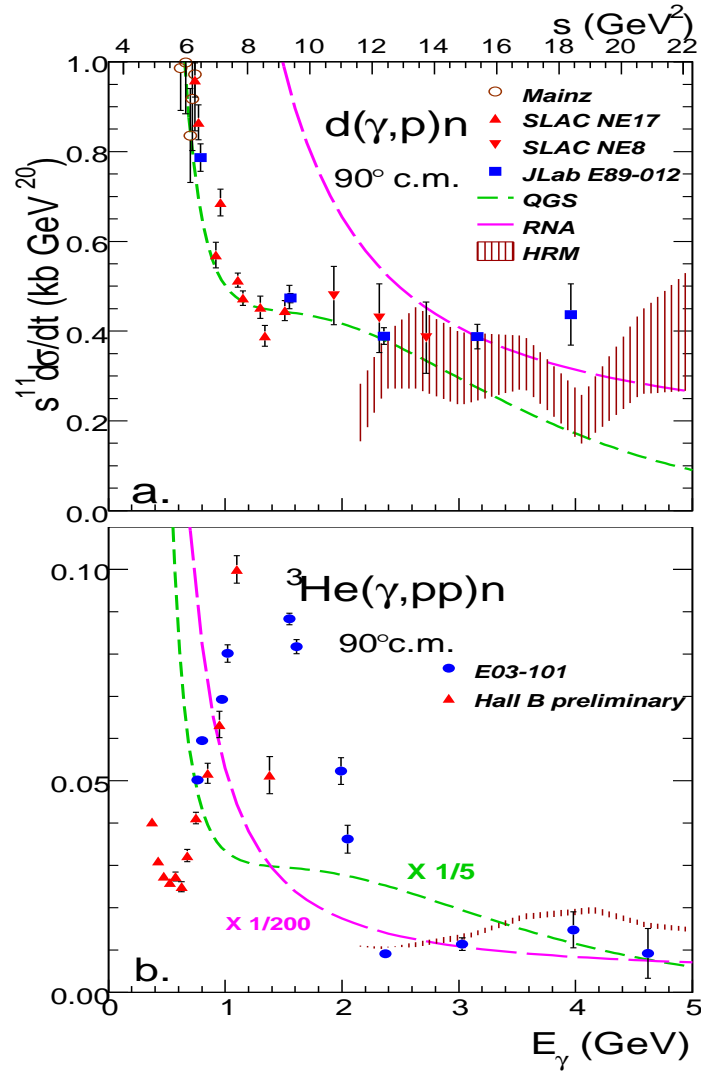


Figure 1: The $d(\gamma, p)n$ (a) and ${}^3\text{He}(\gamma, pp)n$ (b) invariant cross section scaled by s^{11} . ${}^3\text{He}(\gamma, pp)n$ events were selected with $p_n < 100$ MeV/ c . The photon energy bins are 70 (140) MeV for energies up to (above) 2.1 GeV. Model predictions are taken from [25, 30]. In (b), the RNA (QGS) estimate is divided by a factor of 200 (5) to be shown on this scale. Only statistical uncertainties are shown.

- The absolute cross sections in the scaling region indicate strong suppression of pp break-up as compared to that of pn .
- The shape of the scaled cross section in the high photon energy part of the spectrum is tantalizingly similar to the s^{-10} scaling of the hard elastic pp scattering cross section.

Overall, the observation of the s^{-11} scaling for the case of two-proton photodisintegration suggests in a relatively model-independent way that the relevant degrees of freedom that govern the dynamics are the quarks. In a hadronic picture, two-body/one-step processes are strongly suppressed since a charged pion cannot be exchanged between the protons.

However, the simple rescaling of the $d(\gamma, p)n$ RNA and QGS calculations to the ${}^3\text{He}(\gamma, pp)n$ reaction yields rather puzzling results. The RNA formalism [19] after normalization to the deuteron data [30] yields cross sections that are about 200 times larger than the ${}^3\text{He}$ data. The QGS model [27, 28], as estimated in [30], predicts cross sections about a factor of 5 larger than measured.

The HRM prediction agreed with the data only after the observation that some of the helicity conserving amplitudes of pp hard scattering largely cancel while no cancellation exists for the pn amplitude [25].

The disagreement with the RNA prediction however does not completely rule out the scenario in which two protons emerge from pre-existing, high- p_T configurations. This possibility is supported by, for example, the observation of a strong suppression of pp relative to pn two-nucleon correlations [35, 36].

1.4 Second Generation of Hard-Photodisintegration Reactions

The situation discussed in the previous section defines the scope of the measurements that will constitute the “second” generation of the experiment in hard-photodisintegration. The main questions which these experiments will answer are:

1. What is the origin of the large transverse momentum nucleons? Are they pre-existing in the nucleus or are they produced by final state hard rescattering.

2. What accounts for the very low measured cross section ratio of $\gamma^3\text{He} \rightarrow pp + n$ to $\gamma d \rightarrow pn$, which was not anticipated by theory? Is this suppression a property of the nuclear wave function or of nucleon-nucleon hard scattering?
3. Are there oscillations in s^{11} weighted cross section of pp -photodisintegration as there are in s^{10} weighted differential cross section of elastic $pp \rightarrow pp$ scattering.
4. What are the polarization properties of the pp -break-up reaction? Do they have similar anomalies as they were observed in pp hard elastic scattering reactions?
5. What is the origin of the apparent resonance structure in pp breakup at $E_\gamma \leq 2$ Gev?

To realize such a program one needs a simultaneous study of hard photodisintegration of ^3He including breakup of both pp pairs with a neutron spectator and pn pairs with a proton spectator. Extension of such measurements to higher photon-energies will allow checking the prediction of energy oscillations of s^{11} weighted cross sections. The polarization measurements will allow confirmation of the initial observation that the leading quark in the reaction carries the helicity of the incoming photon.

Another new venue for studies of two-nucleon break-up of the ^3He nucleus is utilizing the kinematics of slow recoil nucleon. The measurement of the dependence of the two-nucleon break-up cross section on the light-cone momentum fraction α_n and transverse momentum p_{Tn} of the recoil nucleon provides a new way of checking whether the two large- p_T nucleons originate from the nuclear ground state or are formed due to hard rescattering [30] as well as the role of the two-step/three-body processes in the hard breakup of the two protons [25].

Extension of the hard breakup reaction to the virtual photon electrodisintegration domain will open up completely new area in these studies. The inclusion of the new parameter Q^2 , the photon virtuality, will allow the possibility of reconstructing the impact parameter space in a hard reaction [37] in a similar way to what is currently done for elastic and transition form factors.

Another extension is the consideration of the two high p_T baryons other than nucleons. For example photoproduction of two high- p_T Δ resonances

will probe the hidden-color component of the nuclear ground state wave function [38] if the source of the high p_T baryons is from pre-existing correlations, or it will probe the hard mechanism of $NN \rightarrow \Delta\Delta$ production [39] if the process is due to hard rescattering (a LOI for the measurement of two Δ -isobars photoproduction off the deuteron is also submitted to PAC38).

2 The proposed measurements

We propose a strategy of a step-by-step investigation in which *several short-run-time* experiments will focus on specific aspects of “second” generation measurements.

In this document, we propose to take a 10 days measurement of the $\gamma^3\text{He} \rightarrow pp(n)$ and $\gamma^3\text{He} \rightarrow pn(p)$ reactions at $E_\gamma = 2.2$ GeV. The interpretation of the results is independent of them being taken within the scaling regime. See Appendix B for a description of the differences between this present proposal and the proposal submitted to PAC37.

The proposed measurement will be done in Hall A, using standard Hall A equipment and requiring only a short setup time. The data-taking runs are very short, and may be performed in several intervals, and with poor beam properties. The above conditions make this proposal a candidate 12 GeV commissioning experiment for Hall A.

2.1 The measurement of α_n distribution for ${}^3\text{He}(\gamma, pp)n$ reaction

2.1.1 α_n distribution measurement for ${}^3\text{He}(\gamma, pp)n$

The recoil neutron in $\gamma^3\text{He} \rightarrow pp + n$ gives an additional way to check the underlying mechanism of hard pp pair production. The observable which is best suited for this purpose is the light-cone momentum distribution of the recoil neutron, defined as:

$$\alpha_n = \frac{E_n - p_n^z}{m_{3\text{He}}/3} \quad (1)$$

where E_n and p_n^z are the neutron’s energy and momentum along the z axis respectively (the z direction is chosen in the direction of the incident photon beam).

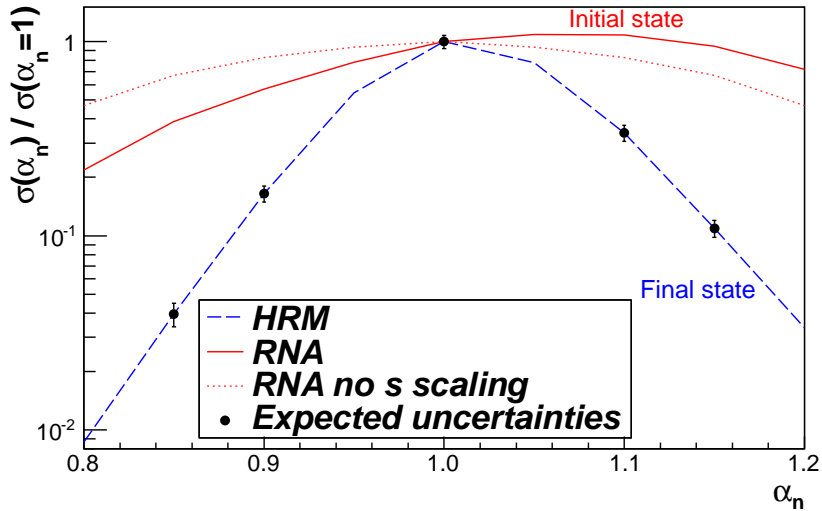


Figure 2: The α_n distribution of the spectator neutron ($p_n < 100$ MeV/c) at $E_e = 2.2$ GeV and $\theta_{cm} = 90^\circ$. The cross section was calculated within the RNA (bold red solid line) and HRM (bold blue dashed line) models. The width of the RNA (HRM) distributions is independent of the exact details of the model but rather represents a feature of an initial state (final state) type calculation. The s dependence of the cross section leads to an asymmetry in the distribution; the RNA model with no s dependence (red dotted line) is shown to indicate the size of the effect. Data points (black dots) are shown on the HRM calculation with uncertainties expected for the proposed beam time. Uncertainties will be smaller if the RNA calculation is correct.

An important feature of high-energy small-angle final-state rescattering is that it does not significantly change the light-cone fractions of the fast protons – see e.g. [40]. As a result, the experimentally determined α_n coincides with the value of α_n in the initial state and measures the light-cone fraction of the two-proton subsystem in the ${}^3\text{He}$ wave function. Furthermore, in the ${}^3\text{He}$ wave function the c.m. momentum distribution of the NN pair depends on the relative momentum of the nucleons in the pair, so one can probe indirectly the magnitude of the momentum in the pp pair involved in the hard disintegration by the measured neutron alpha distribution.

To illustrate the sensitivity of the α_n distribution to the mechanism of the

high- p_T disintegration of a pp pair, we compare in Fig. 2 the α_n dependence of the differential cross section calculated in the framework of the RNA and HRM models. The results presented in Fig. 2 provide substantially different predictions for the α_n distribution. Qualitatively, the much broader distribution of α_n in the RNA model is due to the selection of large momenta of protons in the ${}^3\text{He}$ wave function, which leads to a broader distribution of neutron momenta. In both cases, the simulated data points were generated by sampling the wave function of the neutron in ${}^3\text{He}$ [12] up to 100 MeV/ c .

An important feature of this proposal is that we are not simply asking to determine the α_n distribution in a single kinematics. We first plan to measure and angular distribution of the α_n distribution determining it as a function of the proton transverse momentum for low neutron momentum. The natural expectation is that soft process are relatively larger at forward / backward angles, while hard processes are relatively larger near $\theta_{c.m.} \approx 90^\circ$. Thus we can study how the long- vs. short-range nature of the dynamics change as the process becomes harder.

We second plan to measure the α_n distribution at $\theta_{c.m.} = 90^\circ$ as a function of the transverse momentum of the spectator neutron, p_{Tn} . CLAS data for $\gamma {}^3\text{He} \rightarrow pp + n$ [41] for photon energies near 1 GeV show two distinct peaks in the neutron momentum distribution, a low energy two-body process peak for $p_n \approx 0 - 250$ MeV/ c , and a broad three-body process peak for higher momenta. This p_{Tn} should then show the evolution of α_n with the transition from a three-body to two-body underlying dynamics. While three-body processes are dominant at lower energies, and we expect their suppression with increasing photon energy due to a faster decrease with s , there is no clear evidence about this aside from the s^{-11} behavior seen in E03-101 for low p_n and photon energies above 2 GeV.

2.1.2 ${}^3\text{He}(\gamma, pn)p$

In an attempt to find the reason for the very low magnitude of the cross section ratio:

$$\frac{\frac{d\sigma}{dt}[{}^3\text{He}(\gamma, pp)n]}{\frac{d\sigma}{dt}[d(\gamma, p)n]} \sim 0.025, \quad (2)$$

found in E03-101 [34], we propose to measure the cross section for the break-up of a pn pair out of ${}^3\text{He}$ at various c.m. angles with $E_\gamma = 2.2$ GeV. The proposed data points are plotted in Fig. 3. These measurement will test the various assumptions made by theory about the treatment of pn pairs

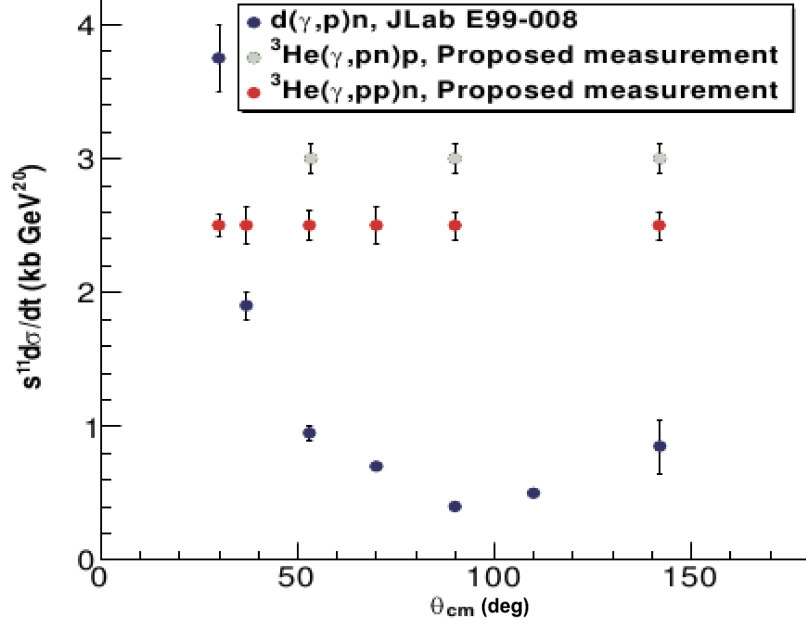


Figure 3: Angular distribution of the invariant cross section scaled with s^{11} for $E_\gamma = 2.2$ GeV. Blue points are the available data for $d(\gamma, p)n$. The proposed measurements for ${}^3\text{He}(\gamma, pn)p$ and ${}^3\text{He}(\gamma, pp)n$ are plotted in gray and red respectively to indicate the angles at which the data are proposed to be taken. The values for the scaled cross sections of the the proposed data were chosen arbitrarily to be shown in this scale.

with a spectator p in ${}^3\text{He}$ vs. a free pn pair (deuteron). If the origin of the high transverse momentum nucleons will be found to be from initial state correlation, then the amount of SRC pp and pn pairs in the ${}^3\text{He}$ w.f. will be directly measured. One can make the following decomposition the cross section ratio:

$$\frac{\sigma[{}^3\text{He}(\gamma, pp)n]}{\sigma[d(\gamma, p)n]} = \frac{\sigma[{}^3\text{He}(\gamma, pp)n]}{\sigma[{}^3\text{He}(\gamma, pn)p]} \times \frac{\sigma[{}^3\text{He}(\gamma, pn)p]}{\sigma[d(\gamma, p)n]}$$

where the first term accounts for the reaction mechanism and the second term accounts for ${}^3\text{He}$ ground state contribution.

In RNA [30] type models, the reaction mechanism relates the pp pair

break-up cross section to pn pair break-up by considering the charge ratio

$$\frac{q_{pp}^2}{q_{pn}^2} = 4,$$

and the form factor ratio

$$\frac{F_p^2 \cdot F_p^2}{F_n^2 \cdot F_p^2} \sim 4$$

to get

$$\frac{\sigma[{}^3\text{He}(\gamma, pp)n]}{\sigma[{}^3\text{He}(\gamma, pn)p]} = \frac{F_p^2}{F_n^2} \cdot \frac{q_{pp}^2}{q_{pn}^2} \cdot R \sim 8.$$

Here R is the the ratio of pp pairs vs pn pairs in ${}^3\text{He}$, evaluated by the RNA model to be $R = \frac{1/3}{2/3} = \frac{1}{2}$.

The cross section ratio

$$\frac{\sigma[{}^3\text{He}(\gamma, pn)p]}{\sigma[d(\gamma, p)n]} = \int^{P_n < 100\text{MeV}/c} |\Psi_{{}^3\text{He}}|^2 d^3p \cdot \frac{2/3}{1} \cdot a_2 \sim \frac{2}{3}$$

is evaluated using ${}^3\text{He}$ wavefunction, while the $\frac{2/3}{1}$ accounts for number of pn pairs in ${}^3\text{He}$ vs pn pairs in d , and $a_2 = 2$ [42, 43] estimates the probability of 2 correlated nucleons in ${}^3\text{He}$ vs. d . This gives an overall estimate based on RNA of

$$\frac{\sigma[{}^3\text{He}(\gamma, pp)n]}{\sigma[d(\gamma, p)n]} = \frac{16}{3}.$$

Since E03-101 results indicate that this cross section ratio is two orders of magnitude lower, every assumption made by theory must be revisited. A direct ${}^3\text{He}(\gamma, pn)p$ measurement will enable us to determine if the discrepancy has to do with our understanding of the process dynamics or with our knowledge of the ${}^3\text{He}$ wavefunction. In particular, the values for R and a_2 will be determined for relative momentum of ~ 2 GeV/ c .

An angular distribution of the ${}^3\text{He}(\gamma, pp)n$ cross section for the same kinematics will also be taken for reference. The rates for both reactions are very high (see Tables 1 and 2) and the required statistics will be gathered in short runs.

3 Experimental details

3.1 Choice of Hall and detectors

The experiment can be performed only in Hall A. Previous measurements of the ${}^3\text{He}(\gamma, pp)n$ reaction in Hall B [44] were limited by statistics to a maximal photon energy of 1.5 GeV. Even the order of magnitude luminosity increase for Hall B with the 12 GeV upgrade is insufficient for adequate statistics.

As discussed below, the full two-body kinematics is done using the measured momenta and angles of the outgoing particles. The resolution in the reconstructed photon energy should be high enough to allow event selection with energy above the pion-production threshold (140 MeV off the bremsstrahlung end-point). This requires momentum and angular resolutions that can be achieved with the two HRSs or one HRS and HAND.

3.2 Experimental overview

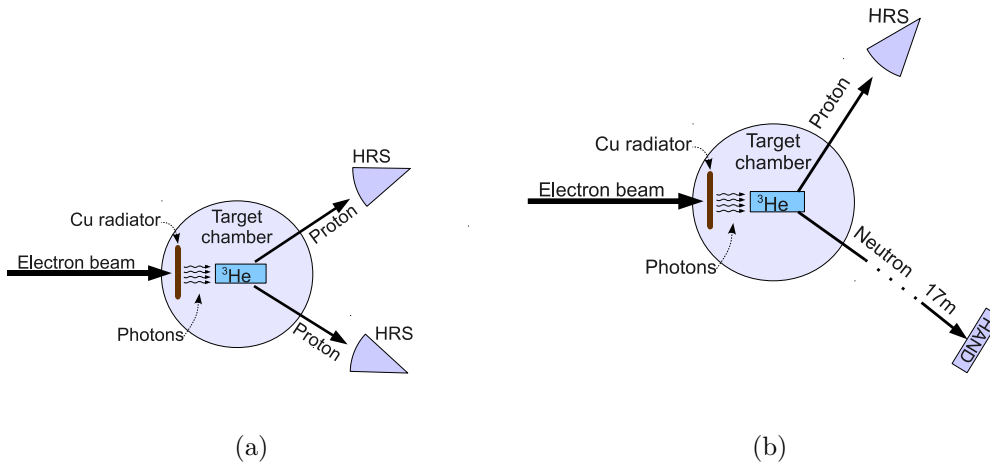


Figure 4: *Experimental setup for the measurement of ${}^3\text{He}(\gamma, pp)n$ (a) and ${}^3\text{He}(\gamma, pn)p$ (b): Bremsstrahlung photons generated in a copper radiator by an electron beam impinge on a ${}^3\text{He}$ gas target. Protons and deuterons are detected with the two HRSs. Neutrons are detected with the neutron array. Elements are not shown to scale.*

We propose to measure $\gamma{}^3\text{He} \rightarrow pp+n_{spec}$ and $\gamma{}^3\text{He} \rightarrow pn+p_{spec}$ in Hall A.

The experimental setup is schematically illustrated in Fig. 4. Bremsstrahlung photons, produced by the electron beam passing through a photon radiator, will impinge on a cryogenic gas ^3He target. The maximum energy of the Bremsstrahlung beam is essentially equal to the incident electron kinetic energy. The target, downstream of the radiator, is irradiated by the photons and the primary electron beam. The experiment will run in two detection modes:

- Detection of two protons in coincidence by the two High Resolution Spectrometers (HRS) (Fig. 4a.).
- Detection of a proton with one HRS in coincidence with a neutron in the n-array (Fig. 4b.).

In the proposed kinematics, each detected particle carries about half the incident beam energy.

3.3 Photon radiator

The radiator is the standard Hall A Cu radiator with a 6% radiation length thickness¹. To limit divergence of the beam and interactions with the target walls and flow diverters, it is preferred to use a radiator foil mounted directly in the cryotarget cell block, about 15 cm upstream of the center of the target. Since the radiator is directly cooled by the cryotarget, melting is not an issue. The main constraint on maximum beam current is the site boundary radiation level. We propose to do the measurement with a 50 μA beam and with the standard cryotarget raster, as has been done in earlier Hall A photodisintegration experiments. The power deposited in the Cu is about 125 W for a beam current of 50 μA .

3.4 Target

We will use the 20-cm long narrow “race track” cryotarget cell, which was used in E03-101. That target has proven to be successful both in reducing the uncertainty associated with the cuts (subtractions of end cap background) and decreasing multiple scattering of the ejected particles, which leads to

¹Although tagged photon beam experiments are generally desirable, the technique is not feasible for high energy, high momentum transfer reactions. The decrease in luminosity makes these small cross sections unmeasurable.

improved momentum and energy resolution. We expect that the target will be able to operate at the same temperature, pressure and density as in the previous run, leading to a ^3He density of 0.079 g/cm^3 .

3.5 High Resolution Spectrometers (HRSs)

We will use the two Hall A spectrometers (HRS_L and HRS_R) to measure the two protons in coincidence. This measurement requires no changes from the standard detector package, electronics and operation of the spectrometers. For this experiment, the spectrometer momentum range is $\approx 1.8 - 3.0 \text{ GeV}/c$ and the angular range is $42^\circ - 53^\circ$ lab. All necessary equipment including detectors, electronics and data acquisition is already available.

3.6 The n-array (HAND)

The Hall A Neutron Detector (HAND) shown in Fig. 5 has been chosen as the neutron detector for two main reasons. First, it is possible to move HAND into and out of position in a short time – HAND is positioned at the same angle for the (γ, pn) measurements as the HRS is for the corresponding (γ, pp) measurements. Second, HAND provides adequate angle and energy resolution for the experiment. HAND was recently reused in experiments E05-102, E08-005 and E07-006 [45–47]. HAND is a large volume neutron detector that consists of 112 plastic scintillator bars, divided up into six planes. Each bar is viewed by two photomultiplier tubes, one on each end. The height of the bars in each of the first three planes is 10 cm, 12.5 cm and 15 cm respectively, and 25 cm for the last three planes. The neutron detector also has a veto detector located in front of the first plane. The veto detector consists of 64 plastic bars that are 2 cm thick and are organized into 32 rows of two end-to-end overlapping paddles. In E07-006 two additional scintillator layers were added. HAND needs a crane to set up. We will be able to cable it so placing it in the proposed kinematics does not require recabling. The kinematic settings have been chosen so there will be no more than one movement of HAND per day, which is expected to take about 4 hours.

For the rate calculations, we simulate HAND as a 3 m (height) \times 1 m (width) detector 17 m from the target. In front of HAND, there will be a shielding wall comprised of lead (1 in thick). The distance between the back face of the wall and the front face of HAND is 56 cm.



Figure 5: *HAND during the E05-102 run, standing at roughly the proposed angle for this measurement. As can be seen in this picture the cables can be placed so the detector can be easily moved. Not shown in the figure is the shielding wall.*

Shielding of HAND from neutrons emitted from the radiator will be done by placing a few meters of cement along the line of sight between the radiator and the detector without obstructing the neutrons emitted from the target. The shielding will decrease the singles seen by the n detector by a factor of 2.

3.7 HCAL

For the purposes of this proposal, we have indicated that we would use HAND as a neutron detector. This choice was made since, first, HAND is an existing detector, second, it satisfies our requirements, and third, the run times are short for the neutron measurements, so the main concern is to have a detector for which the overhead of changing angles is small.

However, a potentially superior option is the hadron calorimeter HCAL being developed as part of the SBS project. HCAL should be a more efficient detector of high-energy neutrons that is less sensitive to backgrounds, since a high energy threshold can be set on it. Assuming HCAL is implemented in a way that keeps the overhead of changing angles small, it would appear perfectly sensible if this experiment runs early in the 12 GeV era for it to use and commission HCAL. We do not see a reason at this point to rule out or absolutely commit to either technology.

3.8 Detection acceptance

The finite acceptance correction for the measurement of coincident pp pairs was determined using the standard Hall A Monte-Carlo simulation software MCEEP [48], and used for the analysis of E03-101 [34, 49].

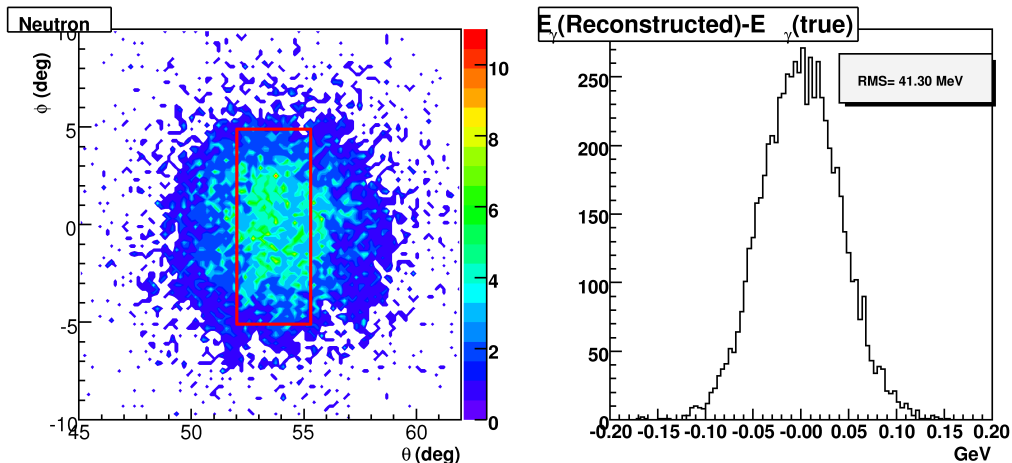


Figure 6: ${}^3\text{He}(\gamma, pn)p$ simulation results. Left: the angular distribution of the emitted neutron in coincidence with a proton detected by the HRS. Events were generated for an $E_e = 2.2$ GeV beam, with bremsstrahlung photon energies above the pion production threshold ($E_e - 140$ MeV). The red box indicates the HAND detector acceptance. Right: the simulated resolution of the reconstructed photon energy.

Another simulation was constructed to evaluate the acceptance and energy resolution for detecting a neutron and a proton in coincidence using

the HAND and the HRS respectively. The left panel of Fig 6 shows the angular distribution of the emitted neutron from the ${}^3\text{He}(\gamma, pn)p$ reaction events in coincidence with a proton detected by the HRS at 53° (90° in the c.m. of the γpn system). The red box indicates the HAND acceptance. The number of accepted events for this case compared to the number of accepted ${}^3\text{He}(\gamma, pp)n$ events (measured by a coincidence between the two HRSs in E03-101), is found to be $\frac{\text{Accept}\{{}^3\text{He}(\gamma, pn)p\}}{\text{Accept}\{{}^3\text{He}(\gamma, pp)n\}} = 1.83$.

3.9 Reconstructed photon energy

The photon energy for each reaction channel can be calculated event by event from the momentum of the detected particles using momentum/energy conservation. To assure that the kinematic reconstruction is valid, one needs to select only two-body events. This selection is done in the same scheme used for E03-101 analysis. The photon energy is calculated assuming a two-body process. Then, only events which are no more than a 140 MeV (pion production threshold) off the bremsstrahlung endpoint are selected. This procedure assures that no third particle can be produced.

The resolution of the reconstructed photon energy in measuring ${}^3\text{He}(\gamma, pp)n$ using the two HRSs was studied in the analysis of E03-101 and found to be in the range of a few MeV. For the ${}^3\text{He}(\gamma, pn)p$ measurement, the expected photon energy resolution was evaluated in the MC by smearing the known angle and momentum of the detected proton and neutron by the measurement resolution and reconstructing the photon energy with the smeared values. The right panel of Fig 6 shows the expected resolution of the reconstructed photon energy. The resolution is found to be $\sigma(E_\gamma) = 41.1$ MeV (r.m.s) which is sufficient to select events which are below the pion production threshold (140 MeV).

3.10 Projected rates

The predicted differential cross sections and expected count rates are shown in Tables 1 and 2. Both the cross sections and count rates have been calculated assuming running conditions of 50 μA current, a 6% copper radiator and the Hall A unpolarized ${}^3\text{He}$ target in the same conditions as in E03-101. For ${}^3\text{He}(\gamma, pp)n$ the cross sections have been calculated based on interpolation from the E03-101 data points. The rates and cross sections for the p_t distribution of the spectator neutron were calculated based on Fig. 6 of [25],

under the assumption of a three-body/two-step process. For the ${}^3\text{He}(\gamma, pn)p$ reaction, rates were estimated using the $d(\gamma, pn)$ cross section [6], taking into account the calculated detection acceptance and the neutron detection efficiency. The neutron detection efficiency for each layer of HAND is about 2%. For 6 layers, taking into account a 50% attenuation by the lead wall [50], we get a total neutron detection efficiency of $D_{eff} = 6\%$. The detection efficiency and attenuation in the lead wall was very recently measured by experiment E07-006. The calculated values will be compared with the E07-006 results once the data is analyzed, to fine tune the rate estimates. Details about the HAND efficiency calculation are in Appendix A.

3.11 Systematic uncertainties

The systematic uncertainties involved in the cross section calculation were thoroughly studied in the analysis of E03-101. They are dominated by:

- The background subtraction of electroproduction events, which requires an estimation of the number of Bremsstrahlung photons per electron taken from theory [51].
- The evaluation of the acceptance for detecting the two protons into the two HRS in coincidence, which is done by simulation. The simulation depends on the wave function of the spectator neutron taken from theory.

The total systematic uncertainty in the cross section is estimated to be less than 7% for the proposed kinematics.

3.12 Random coincidence rate calculation

The ${}^3\text{He}(\gamma, pp)n$ data from E03-101 shows that the contamination of the data by random proton and deuteron accidentals is negligible because the singles rates of high-energy protons and deuterons in the HRS is small. For the ${}^3\text{He}(\gamma, pn)p$ channel, the random coincidence rate is calculated in appendix A. The optimized detection threshold was found to be 20-50 MeVee. For the proposed run times, this rate will introduce a $\sim 10\%$ statistical uncertainty at most for all ${}^3\text{He}(\gamma, pn)p$ data points.

Table 1: *Estimated cross sections, rates, requested beam time and kinematic setup for the ${}^3\text{He}(\gamma,pp)n$ α_n and p_{Tn} distribution measurements.*

#	θ_{cm}	α_n	p_{Tn}	θ_{HRS-L}	P_{HRS-L}	θ_{HRS-R}	P_{HRS-R}	$\frac{d\sigma}{d\Omega}$	Rate	Yield	Time
	[deg]		$[\frac{MeV}{c}]$	[deg]	$[\frac{GeV}{c}]$	[deg]	$[\frac{GeV}{c}]$	$[\frac{pb}{GeV^2}]$	$[\frac{cnt}{Hr}]$	# evts	Hrs
1	30	1.15	0	14.78	2.720	105.68	0.720	10.8	102	102	1
2	30	1.10	0	15.03	2.705	109.69	0.745	33.6	316	316	1
3	30	1.00	0	15.57	2.676	117.75	0.812	99.4	935	935	1
4	30	0.90	0	16.19	2.646	125.68	0.908	16.4	154	154	1
5	30	0.85	0	16.53	2.630	129.54	0.970	3.9	37	111	3
The measurements above are consistent with $\theta_{HAND} = 86.30^\circ$											
6	37	1.15	0	18.36	2.651	96.07	0.840	6.4	60	120	2
7	37	1.10	0	18.67	2.637	99.57	0.856	19.8	186	186	1
8	37	1.00	0	19.34	2.610	106.91	0.904	58.5	551	551	1
9	37	0.90	0	20.11	2.582	114.61	0.976	9.7	91	91	1
10	37	0.85	0	20.53	2.568	118.55	1.025	2.3	22	109	5
The measurements above are consistent with $\theta_{HAND} = 86.30^\circ$											
11	53	1.15	0	26.91	2.448	78.75	1.130	3.8	36	107	3
12	53	1.10	0	27.36	2.438	81.13	1.134	11.7	110	110	1
13	53	1.00	0	28.34	2.417	86.36	1.150	34.7	326	326	1
14	53	0.90	0	29.46	2.396	92.31	1.179	5.7	54	108	2
15	53	0.85	0	30.07	2.385	95.59	1.201	1.4	13	103	8
The measurements above are consistent with $\theta_{HAND} = 52.53^\circ$											
16	70	1.15	0	36.78	2.177	64.26	1.447	2.8	26	104	4
17	70	1.10	0	37.39	2.171	65.76	1.446	8.6	81	162	2
18	70	1.00	0	38.72	2.158	69.07	1.445	25.4	239	239	1
19	70	0.90	0	40.22	2.147	72.90	1.450	4.2	40	119	3
20	70	0.85	0	41.05	2.141	75.06	1.456	1.0	9	95	10
The measurements above are consistent with $\theta_{HAND} = 52.53^\circ$											
21	90	1.15	0	49.95	1.812	49.95	1.812	1.8	17	104	6
22	90	1.10	0	50.78	1.811	50.78	1.811	5.7	54	108	2
23	90	1.00	0	52.56	1.809	52.56	1.809	17.0	160	319	2
24	90	0.90	0	54.55	1.811	54.55	1.811	2.8	26	105	4
25	90	0.85	0	55.64	1.813	55.64	1.813	0.7	6	101	16
The measurements above are consistent with $\theta_{HAND} = 19.88^\circ$											
26	142	1.15	0	101.00	0.870	19.56	2.551	6.2	59	117	2
27	142	1.10	0	102.47	0.885	19.68	2.565	19.3	181	181	1
28	142	1.00	0	105.47	0.918	19.89	2.600	57.0	537	537	1
29	142	0.90	0	108.60	0.958	20.05	2.649	9.4	89	177	2
30	142	0.85	0	110.23	0.982	20.11	2.680	2.3	21	106	5
The measurements above are consistent with $\theta_{HAND} = 19.88^\circ$											
31	90	1.15	100	49.12	1.902	50.92	1.724	1.9	18	105	6
32	90	1.10	100	49.92	1.900	51.77	1.723	5.8	54	109	2
33	90	1.00	100	51.66	1.897	53.59	1.724	17.1	161	322	2
34	90	0.90	100	53.61	1.896	55.62	1.728	2.8	27	106	4
35	90	0.85	100	54.67	1.897	56.73	1.731	0.7	6	102	16
The measurements above are consistent with $\theta_{HAND} = 19.88^\circ$											
36	90	1.15	200	48.40	1.994	52.03	1.638	2.0	19	115	6
37	90	1.10	200	49.19	1.991	52.90	1.639	6.3	59	119	2
38	90	1.00	200	50.89	1.986	54.76	1.642	18.6	175	351	2
39	90	0.90	200	52.79	1.983	56.82	1.648	3.1	29	116	4
40	90	0.85	200	53.83	1.982	57.95	1.652	0.7	7	111	16
The measurements above are consistent with $\theta_{HAND} = 19.88^\circ$											
41	90	1.15	300	47.80	2.088	53.29	1.555	3.7	35	104	3
42	90	1.10	300	48.57	2.083	54.17	1.557	11.5	108	108	1
43	90	1.00	300	50.23	2.076	56.07	1.562	33.9	319	319	1
44	90	0.90	300	52.08	2.071	58.17	1.570	5.6	53	105	2
45	90	0.85	300	53.11	2.070	59.32	1.576	1.3	13	101	8
										Total:	168

Table 2: *Estimated cross sections, rates, requested beam time and kinematic setup for the ${}^3\text{He}(\gamma, pn)p$ angular distribution measurements.*

θ_{cm}	θ_{HRS-L}	P_{HRS-L}	θ_{HAND}	P_{HAND}	$\frac{d\sigma}{dt}$	Rate	Yield	Time
[deg]	[deg]	$[\frac{\text{GeV}}{c}]$	[deg]	$[\frac{\text{GeV}}{c}]$	$[\frac{\text{pb}}{\text{GeV}^2}]$	$[\frac{\text{cnt}}{\text{Hr}}]$	# evts	Hrs
142	105.43	0.917	19.88	2.599	720	760	760	1
90	52.54	1.808	52.53	1.808	340	360	720	2
53	28.33	2.415	86.30	1.149	800	840	840	1
							Total:	4

4 Kinematics and requested beam time

The kinematic settings are listed in tables 1 and 2. The proposed data points and expected statistical uncertainties are plotted in Figures 2 and 3. The kinematic settings were selected to match the available $d(\gamma, p)n$ data. The cross sections and count rates have been calculated based on interpolation from JLab E03-101 and E99-008 data, assuming 50 μA current, a 6% copper radiator and the Hall A unpolarized ${}^3\text{He}$ target.

With the proposed kinematics, HAND will be moved once per day. This will allow us to take many short measurements in the different kinematics listed in Table 1 with no need to move HAND from one side of HRS-R to another. One may observe from Table 1, that kinematic settings #1 - #25 can be taken with the different floor angles proposed for HAND. After these measurements HAND may be taken out of the Hall,

The beam time request is summarized in Table 3 for a total of 10 days.

5 Summary

We propose to take high energy data for the ${}^3\text{He}(\gamma, pp)n$ and ${}^3\text{He}(\gamma, pn)p$ reactions in high momentum-transfer kinematics. An α_n distribution measurement for ${}^3\text{He}(\gamma, pp)n$ will enable us to determine whether the underlying mechanism of hard NN pair production is *initial state correlation* or *final state rescattering*. A p_{Tn} distribution measurement of the spectator neutron will allow us to evaluate the contribution of a three-body/two-step mecha-

Table 3: *Summary of the requested beam time.*

Measurement	Time [days]
Setup & Checkout	1
Measurement at 2.2 GeV on ^3He target 48 Kinematic changes 3 movements of HAND, scheduled one per day	9
TOTAL REQUESTED BEAM TIME	10

nism to this process. The interpretation does not rely on being in the scaling regime. The direct measurement of the hard pp to np pair production out of ^3He will enable us to find the origin for the unexplained low magnitude of the $\frac{d\sigma}{dt}[^3\text{He}(\gamma,pp)n]$ ratio found in previous measurements.

Appendix A: ${}^3\text{He}(\gamma, pn)p$ Random coincidence rate calculation

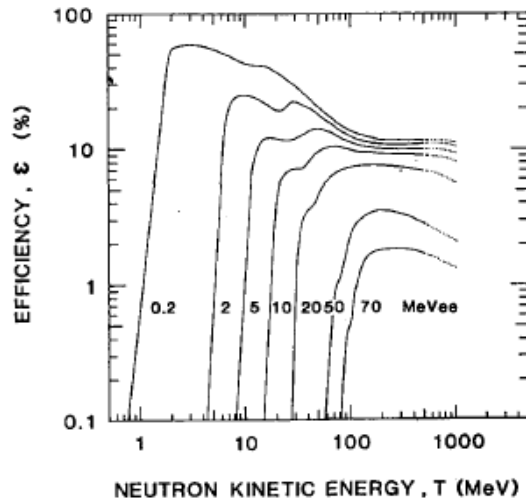


Figure 7: Neutron detection efficiencies calculated with the code of Cecil *et al.* [52]. Detector pulse-height thresholds are given in MeV equivalent electron energy (MeV *ee*). Taken from [53].

The uncertainty involved with subtracting random coincidence events can be minimized by placing an optimal detection threshold on HAND. Fig. 7 (taken from [53]) shows the detection efficiency for a 10 cm plastic scintillator for different threshold values in the range of 0.2 – 70 MeV equivalent electron (MeV_{ee}), calculated with the code of Cecil *et al.* [52]. HAND consists of 6 scintillator planes, each with 10 cm width, which yields an overall efficiency of:

$$\epsilon_{HAND} = 0.5 \cdot (1 - (1 - \epsilon_n)^6), \quad (3)$$

where 0.5 is the expected attenuation of the lead wall (see Sec. 3.10) and ϵ_n is the single scintillator plane efficiency taken from Fig. 7.

In order to evaluate p-n accidental detection rates, we first evaluate proton and neutron singles rates for the proposed luminosity. The proton singles rate was measured in E03-101 at $E_{beam}=2.1$ GeV with the same kinematics.

Scaling this measured rate to a current of $50 \mu\text{A}$ gives:

$$\dot{N}_p(\text{proposed}) = 1.4 \text{ kHz} \quad (4)$$

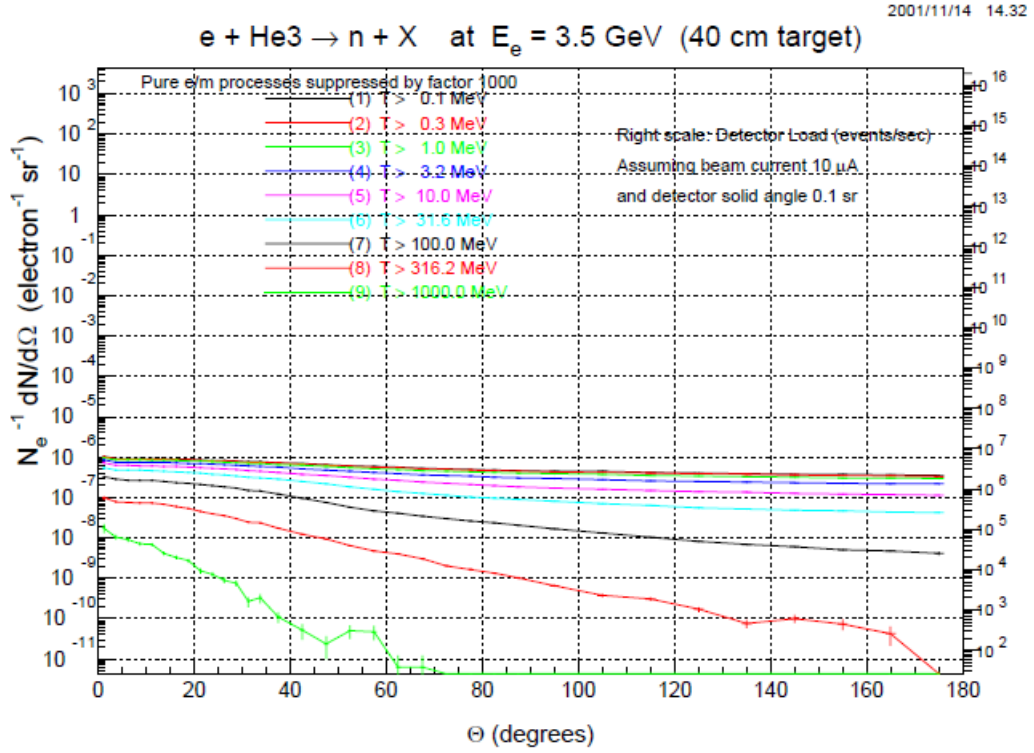


Figure 8: *The neutron singles yield with kinetic energy above given thresholds. Calculated in [54, 55].*

To evaluate the neutron singles rate, we use a calculation by Degtyarenko [54, 55] of $e + {}^3\text{He} \rightarrow n + X$ rates, as shown in Fig. 8. For 55° , we calculate the neutron singles rates ($\dot{N}_n(\text{Degtyarenko})$) as a function of the minimal kinetic energy of the detected neutron. The latter is determined from Fig. 7 as a function of the threshold. The values in Fig. 8 are given for a solid angle of 100 msr, and nucleon luminosity of

$$L(\text{Degtyarenko}) = 5 \cdot 10^{36} \text{ cm}^{-2}\text{sec}^{-1}. \quad (5)$$

Table 4: *Cryotarget nucleon luminosity for 50 μ A beam.*

	Thickness (cm)	Density (gr/cm ³)	Luminosity for I=50 μ A (sec ⁻¹ cm ⁻²)
Entrance window (Al)	0.0347	2.81	$1.8 \cdot 10^{37}$
Exit window (Al)	0.0300	2.81	$1.6 \cdot 10^{37}$
³ He	20	0.079	$3.0 \cdot 10^{38}$
Total			$3.3 \cdot 10^{38}$

Table 4 summarizes the luminosity of the ³He cryotarget we plan to use. The total luminosity of the target is

$$L(\text{proposed}) = 3.3 \cdot 10^{38} \text{ cm}^{-2}\text{sec}^{-1} \quad (6)$$

The solid angle of the HAND detector at the proposed 17 m is:

$$\Delta\Omega_n(\text{proposed}) = \frac{A_{HAND}}{A_{4\pi}} = \frac{1 \text{ m} \cdot 3 \text{ m}}{(17 \text{ m})^2} = 10 \text{ msr} \quad (7)$$

Using this information we can now scale the rates of [54, 55] to obtain an estimate for the singles rate of the proposed setup:

$$\dot{N}_n(\text{proposed}) = \dot{N}_n(\text{Degtyarenko}) \cdot \epsilon_{HAND} \cdot \frac{L(\text{proposed})}{L(\text{Degtyarenko})} \cdot \frac{\Delta\Omega_n(\text{proposed})}{\Delta\Omega(\text{Degtyarenko})} \quad (8)$$

The np random coincidence rate can now be estimated as:

$$\dot{N}_{Random} = \dot{N}_p \cdot \dot{N}_n \cdot t_{resolv} \quad (9)$$

Table 5 shows the random coincidence uncertainty calculation for different values of pulse-height detection threshold. The values are calculated for the 90° c.m. data point which has the lowest projected rate of all the proposed $\gamma^3\text{He} \rightarrow pn$ data points, under the assumption of 2 hours of beam time. The resolving time is taken to be 2 ns.

For a threshold value of 50 MeVee, with the expected signal rate and available beam time (determined by other considerations) we expect to measure the $^3\text{He}(\gamma, pn)p$ cross section with statistical uncertainty better than 10% at all proposed kinematics.

Table 5: The rates and statistical uncertainty for the ${}^3\text{He}(\gamma, pn)p$ measurement. The calculation is given for different values of detection threshold. The threshold value of choice is highlighted.

Thres- hold	T_n thres- hold	Plane eff (ϵ_n)	HAND eff (ϵ_{HAND})	pn Co- inc. rate	p sin- gles rate	n sin- gles rate	Rndm. coinc. rate	Signal events (S)	Rndm. events (N)	$\frac{\sqrt{S+2N}}{S}$
MeVee	MeV	%	%	Hz	kHz	kHz	Hz	Cnts	Cnts	%
0.2	1	12	27	0.46	1.4	6400	18	3300	130000	15
2	6	10	23	0.4	1.4	4800	13	2900	97000	15
5	12	9	22	0.37	1.4	3700	10	2600	75000	15
10	20	8	20	0.34	1.4	2700	7.6	2400	54000	14
20	40	5.5	14	0.25	1.4	1500	4.1	1800	30000	14
50	80	2	5.7	0.097	1.4	78	0.22	700	1600	8.9
70	120	1.2	3.5	0.06	1.4	72	0.2	430	1400	13

Comment: For the detection of 1-2 GeV/c neutrons a better neutron detection is possible by introducing absorbers between the scintillators, as was done in BigHand for the GEn measurement [56]. In our case the limiting factor is the necessity to move the detector to a few positions. The calculation given here shows that for the projected rates, beam time, and neutron energies of the proposed measurement, the current HAND detector is sufficient.

Appendix B: Response to the PAC37's Concern

From the PAC37 Draft Report: “**Issues:** *The primary focus of this experiment is the comparison of the pp hard photodisintegration cross section at gamma ray energies of 3 and 4.4 GeV. To be conclusive it will be necessary to demonstrate that these measurements are safely in the scaling regime. The earlier huge discrepancies for pp hard photodisintegration between expectations and the results of the previous experiment E-03-101 were meanwhile significantly reduced based on new calculations. To further explore this the collaboration proposed to measure in addition to pp channel the pn channel. This, the study of the cross section as a function of alpha, and the study of the ${}^3\text{He}$ disintegration into d-p pairs at high Q^2 does add additional motivation for the measurements, however, the committee is not convinced that the proposed measurements with limited kinematic coverage will lead to a clear picture of the hard photodisintegration mechanism in the scaling regime. Therefore, it does not meet the criteria for approval for the top half of the first 5 years of 12 GeV operation.*”

The main concern of PAC37 was that the limited kinematic coverage proposed for the ${}^3\text{He}(\gamma, pp)n$, ${}^3\text{He}(\gamma, pn)p$ and ${}^3\text{He}(\gamma, dp)$ reactions would not allow a clear interpretation of the underlying dynamics responsible for the unexpected observations from E03-101.

For the present proposal we have substantially revised our strategy. First, we now propose a step-by-step approach in which we focus on a limited number of issues in dedicated short run-time experiments, rather than addressing several unresolved aspects of hard photodisintegration within one experiment. Since the domain of nuclear reactions beyond the limits of the meson-baryon picture is essentially uncharted, previous experience tells us that each new experiment has a large potential “surprise” factor in it. Therefore we consider the step-by-step approach as the most economical way to progress in the field.

Second, for this first step we have proposed a set of measurements that have a clean interpretation about general aspects of the reaction mechanism, independent of the details of the various calculations, or even whether we are fully within the scaling regime. We expect the p_{Tn} (recoil neutron p_T) distributions to exhibit a transition from two-body dynamics at low p_{Tn} to three-body dynamics at high p_{Tn} . The angular distribution gives a depen-

dence on p_{Tp} (proton p_T), which we expect to vary from forward-angle soft physics to large-angle hard physics, as evidenced by the s -dependence. We expect the α_n distribution to reflect whether the dynamics are sensitive to the long- vs. short-range structure of the nucleus, through the width of the distribution, and to reflect the s -dependence of the reaction, indicating if the data are in the scaling regime, through the asymmetry of the distribution. The study of α_n is done both as a function of p_{Tp} and p_{Tn} , allowing its evolution to be determined. These features are studied through measurements of ${}^3\text{He}(\gamma, pp)n$. With measurements of ${}^3\text{He}(\gamma, pn)p$, we expect to be able to separate out the nuclear structure vs. reaction dynamics aspects that account for the very different cross sections for γpp vs. γpn disintegration.

Table 6 lists the differences between the present proposal and the one submitted to PAC37.

Table 6: Differences between the present proposal and the proposal submitted to PAC37

Reaction	Observable	Motivation	PAC 37	PAC 38
${}^3\text{He}(\gamma, pp)n$	α_n at $\theta_{cm} = 90^\circ$	Final state vs. Initial state	Yes	Yes
	Angular dependence of α_n	Onset of hard dynamics	No	Yes
	p_{Tn} (spectator) dependence of α_n	Evidence for 2-body/3-step dominated dynamics	No	Yes
	Energy dependence of $\frac{d\sigma}{dt}$	Deviation from scaling	Yes	No
${}^3\text{He}(\gamma, pn)p$	Angular dependence of $\frac{d\sigma}{dt}$	Resolve the low magnitude of $\frac{\gamma \rightarrow pp}{\gamma \rightarrow pn}$ issue	Yes	Yes
${}^3\text{He}(\gamma, dp)$	Energy dependence of $\frac{d\sigma}{dt}$	Scaling law validation	Yes	No

References

- [1] J. Napolitano et al. Measurement of the differential cross-section for the reaction $H-2(\gamma, p)n$ at high photon energies and $\theta(\text{c.m.}) = 90^\circ$. *Phys. Rev. Lett.*, 61:2530–2533, 1988.
- [2] S. J. Freedman et al. Two-body disintegration of the deuteron with 0.8-GeV to 1.8-GeV photons. *Phys. Rev.*, C48:1864–1878, 1993.
- [3] J. E. Belz et al. Two body photodisintegration of the deuteron up to 2.8- GeV. *Phys. Rev. Lett.*, 74:646–649, 1995.
- [4] C. Bochna et al. Measurements of deuteron photodisintegration up to 4.0- GeV. *Phys. Rev. Lett.*, 81:4576–4579, 1998.
- [5] E. C. Schulte et al. Measurement of the high energy two-body deuteron photodisintegration differential cross-section. *Phys. Rev. Lett.*, 87:102302, 2001.
- [6] E. C. Schulte et al. High energy angular distribution measurements of the exclusive deuteron photodisintegration reaction. *Phys. Rev.*, C66:042201, 2002.
- [7] M. Mirazita et al. Complete angular distribution measurements of two-body deuteron photodisintegration between 0.5-GeV and 3-GeV. *Phys. Rev.*, C70:014005, 2004.
- [8] P. Rossi et al. Onset of asymptotic scaling in deuteron photodisintegration. *Phys. Rev. Lett.*, 94:012301, 2005.
- [9] H. Arenhoevel, E. M. Darwish, A. Fix, and M. Schwamb. Present status of electromagnetic reactions on the deuteron above pion threshold. *Mod. Phys. Lett.*, A18:190–199, 2003.
- [10] Michael Schwamb and Hartmuth Arenhovel. Offshell effects in electromagnetic reactions on the deuteron. *Nucl. Phys.*, A696:556–580, 2001.
- [11] Michael Schwamb and Hartmuth Arenhovel. The role of meson retardation in the NN interaction above pion threshold. *Nucl. Phys.*, A690:647–681, 2001.

- [12] R. Schiavilla. Induced Polarization in the ${}^2\text{H}(\gamma, \vec{n}){}^1\text{H}$ Reaction at Low Energy. *Phys. Rev.*, C72:034001, 2005.
- [13] Stanley J. Brodsky and Benson T. Chertok. Deuteron form factor and the short-distance behavior of the nuclear force. *Phys. Rev. Lett.*, 37(5):269–272, Aug 1976.
- [14] Stanley J. Brodsky and Benson T. Chertok. Asymptotic form factors of hadrons and nuclei and the continuity of particle and nuclear dynamics. *Phys. Rev. D*, 14(11):3003–3020, Dec 1976.
- [15] Stanley J. Brodsky and Glennys R. Farrar. Scaling Laws at Large Transverse Momentum. *Phys. Rev. Lett.*, 31:1153–1156, 1973.
- [16] V. A. Matveev, R. M. Muradian, and A. N. Tavkhelidze. Automodellism in the large - angle elastic scattering and structure of hadrons. *Nuovo Cim. Lett.*, 7:719–723, 1973.
- [17] K. Wijesooriya et al. Polarization measurements in high-energy deuteron photodisintegration. *Phys. Rev. Lett.*, 86:2975–2979, 2001.
- [18] X. Jiang et al. Recoil-Proton Polarization in High-Energy Deuteron Photodisintegration with Circularly Polarized Photons. *Phys. Rev. Lett.*, 98:182302, 2007.
- [19] Stanley J. Brodsky and John R. Hiller. Reduced nuclear amplitudes in quantum chromodynamics. *Phys. Rev.*, C28:475, 1983.
- [20] S.J. Brodsky, J.R. Hiller, Chueng-Ryong Ji, and G.A. Miller. Perturbative QCD and factorization of coherent pion photoproduction on the deuteron. *Phys.Rev.*, C64:055204, 2001.
- [21] A.E.L. Dieperink and S.I. Nagorny. Photodisintegration of the deuteron in the few GeV region using asymptotic amplitudes. *Phys.Lett.*, B456:9–15, 1999.
- [22] N.A. Khokhlov, V.A. Knyr, and V.G. Neudatchin. Nucleon-nucleon wave function with short-range nodes and high-energy deuteron photodisintegration. *Phys.Rev.*, C75:064001, 2007.

- [23] Leonid L. Frankfurt, Gerald A. Miller, Misak M. Sargsian, and Mark I. Strikman. QCD rescattering and high energy two-body photodisintegration of the deuteron. *Phys. Rev. Lett.*, 84:3045–3048, 2000.
- [24] Misak M. Sargsian. Polarization Observables in Hard Rescattering Mechanism of Deuteron Photodisintegration. *Phys. Lett.*, B587:41–51, 2004.
- [25] Misak M. Sargsian and Carlos Granados. Hard Break-Up of Two-Nucleons from the ^3He Nucleus. *Phys. Rev.*, C80:014612, 2009.
- [26] V.Yu. Grishina, L.A. Kondratyuk, W. Cassing, E. De Sanctis, M. Mirazita, et al. Forward-backward angle asymmetry and polarization observables in high-energy deuteron photodisintegration. *Eur. Phys. J.*, A19:117–123, 2004.
- [27] V.Yu. Grishina, L.A. Kondratyuk, W. Cassing, A.B. Kaidalov, E. De Sanctis, et al. Deuteron photodisintegration within the quark gluon strings model and QCD motivated nonlinear Regge trajectories. *Eur. Phys. J.*, A10:355–364, 2001.
- [28] V.Yu. Grishina, L.A. Kondratyuk, W. Cassing, E. De Sanctis, M. Mirazita, et al. Polarization observables in high-energy deuteron photodisintegration within the quark gluon strings model. *Eur. Phys. J.*, A18:207–209, 2003.
- [29] M. Sargsian. private communication.
- [30] S. J. Brodsky et al. Hard photodisintegration of a proton pair in He-3. *Phys. Lett.*, B578:69–77, 2004.
- [31] G. Peter Lepage and Stanley J. Brodsky. Exclusive Processes in Perturbative Quantum Chromodynamics. *Phys. Rev.*, D22:2157, 1980.
- [32] Joseph Polchinski and Matthew J. Strassler. Hard scattering and gauge / string duality. *Phys. Rev. Lett.*, 88:031601, 2002.
- [33] Ronald Gilman and Franz Gross. Electromagnetic structure of the deuteron. *J. Phys.*, G28:R37–R116, 2002.
- [34] I. Pomerantz et al. Hard photodisintegration of a proton pair. *Physics Letters B*, 684(2-3):106 – 109, 2010.

- [35] E. Piasetzky, M. Sargsian, L. Frankfurt, M. Strikman, and J. W. Watson. Evidence for the Strong Dominance of Proton-Neutron Correlations in Nuclei. *Phys. Rev. Lett.*, 97:162504, 2006.
- [36] R. Subedi et al. Probing Cold Dense Nuclear Matter. *Science*, 320:1476–1478, 2008.
- [37] Paul Hoyer and Samu Kurki. Measuring transverse shape with virtual photons. *Phys. Rev. D*, 83(11):114012, Jun 2011.
- [38] Stanley J. Brodsky and Chueng-Ryong Ji. Factorization property of the deuteron. *Phys. Rev. D*, 33(9):2653–2659, May 1986.
- [39] Carlos G. Granados and Misak M. Sargsian. Hard breakup of the deuteron into two δ isobars. *Phys. Rev. C*, 83(5):054606, May 2011.
- [40] Misak M. Sargsian. Selected topics in high energy semi-exclusive electro-nuclear reactions. *Int. J. Mod. Phys.*, E10:405–458, 2001.
- [41] S. Niccolai et al. Complete measurement of three-body photodisintegration of He-3 for photon energies between 0.35-GeV and 1.55-GeV. *Phys. Rev.*, C70:064003, 2004.
- [42] A. Nogga, H. Kamada, and W. Glöckle. Solution of the faddeev-yakubovsky equations using realistic nn and 3n interactions. *Nuclear Physics A*, 689(1-2):357 – 360, 2001.
- [43] J. L. Forest, V. R. Pandharipande, Steven C. Pieper, R. B. Wiringa, R. Schiavilla, and A. Arriaga. Femtometer toroidal structures in nuclei. *Phys. Rev. C*, 54(2):646–667, Aug 1996.
- [44] S. Strauch. private communication.
- [45] S. Gilad et al. JLab proposal PR05-102:Measurements of Ax and Az Asymmetries in the Quasi-elastic $^3\text{He}(e,e'd)$ Reaction.
- [46] T. Averett et al. Jlab proposal pr08-005: Measurement of the target single-spin asymmetry, ay, in the quasi-elastic $^3\text{he}(e,e'n)$ reaction.
- [47] S. Gilad et al. Jlab proposal pr07-006: Studying short-range correlations in nuclei at the repulsive core limit via the triple coincidence $(e,e'pn)$ reaction.

- [48] P. E. Ulmer. Mceep: Monte carlo for electro-nuclear coincidence experiments. 1991. CEBAF-TN-91-101.
- [49] I. Pomerantz, Y.Ilieva, et al. to be submitted for publication, Phys. Rev. Lett.
- [50] R. Subedi. Ph.d thesis, kent state university, (2007);.
- [51] L. Tiator and L. E. Wright. Virtual photons in pion electroproduction. *Nucl. Phys.*, A379:407–414, 1982.
- [52] R. A. Cecil, B. D. Anderson, and R. Madey. Improved predictions of neutron detection efficiency for hydrocarbon scintillators from 1 mev to about 300 mev. *Nuclear Instruments and Methods*, 161(3):439–447, 1979.
- [53] R. Madey, J.W. Watson, M. Ahmad, B.D. Anderson, A.R. Baldwin, A.L. Casson, W. Casson, R.A. Cecil, A. Fazely, J.M. Knudson, C. Lebo, W. Pairsuwan, P.J. Pella, J.C. Varga, and T.R. Witten. Large volume neutron detectors with subnanosecond time dispersions. *Nuclear Instruments and Methods in Physics Research*, 214(2-3):401 – 413, 1983.
- [54] P. Degtyarenko. Applications of the photonuclear fragmentation model to radiation protection problems. CEBAF-PR-95-66.
- [55] P. Degtyarenko, M. Kossov, and H. Wellisch. Chiral invariant phase space event generator. *The European Physical Journal A - Hadrons and Nuclei*, 8:217–222, 2000. 10.1007/s100500070108.
- [56] B. Wojtsekhowski et al. JLab proposal PR02-013: Measurement of the Neutron Electric Form Factor G_En at High Q².